Environ Sci Pollut Res (2017) 24:21710–21720
DOI 10.1007/s11356-017-9804-9

RESEARCH ARTICLE

Pyrite oxidation under simulated acid rain weathering conditions

Kai Zheng[1,2] · **Heping Li**[1] · **Luying Wang**[1,2] · **Xiaoying Wen**[1,2] · **Qingyou Liu**[1]

Received: 4 January 2017 / Accepted: 20 July 2017 / Published online: 31 July 2017

Abstract We investigated the electrochemical corrosion behavior of pyrite in simulated acid rain with different acidities and at different temperatures. The cyclic voltammetry, polarization curve, and electrochemical impedance spectroscopy results showed that pyrite has the same electrochemical interaction mechanism under different simulated acid rain conditions, regardless of acidity or environmental temperature. Either stronger acid rain acidity or higher environmental temperature can accelerate pyrite corrosion. Compared with acid rain having a pH of 5.6 at 25 °C, the prompt efficiency of pyrite weathering reached 104.29% as the acid rain pH decreased to 3.6, and it reached 125.31% as environmental temperature increased to 45 °C. Increasing acidity dramatically decreases the charge transfer resistance, and increasing temperature dramatically decreases the passivation film resistance, when other conditions are held constant. Acid rain always causes lower acidity mine drainage, and stronger acidity or high environmental temperatures cause serious acid drainage. The natural parameters of latitude, elevation, and season have considerable influence on pyrite weathering, because temperature is an important influencing factor. These experimental results are of direct significance for the assessment and management of sulfide mineral acid drainage in regions receiving acid rain.

Responsible editor: Philippe Garrigues

✉ Qingyou Liu
liuqingyou@vip.gyig.ac.cn

[1] Key Laboratory of High-temperature and High-pressure Study of the Earth's Interior, Institute of Geochemistry, Chinese Academy of Sciences, Guiyang 550002, China

[2] University of Chinese Academy of Sciences, Beijing 100039, China

Keywords Pyrite · Simulated acid rain · Weathering · pH drainage

Introduction

Pyrite is the most abundant terrestrial sulfide mineral occurring in the Earth's crust (Peters and Majima 1968). During natural geochemical processes or human mineral extraction exploitation, pyrite can easily be oxidized, causing environmental issues or affecting its use in industrial applications. Hence, researchers have concentrated on its oxidizing behavior. Very large numbers of studies have reported on pyrite's industrial processes and applications, which include industrial mineral beneficiation processes, such as noble metal flotation (Ivanova et al. 2015; Rabieh et al. 2016) and leaching (Nicol 2016; Mitsunobu et al. 2016), sensors (Stanić and Dimić 2013; Simic et al. 2010; Mihajlović et al. 2009), and fuel cells (Reinholz et al. 2016; Xiao et al. 2013).

Under natural conditions, pyrite occurs as raw ore and mining industry waste rocks and tailings. When exposed to air and water, it undergoes atmospheric and aqueous oxidation, which is the so-called weathering phenomenon in geology. It then releases elemental S, polysulfide, and Fe^{3+} oxidized species (Donato et al. 1993) and ultimately causes acid mine drainage (AMD). Moreover, pyrite often accompanies other sulfides, coal, and uranium ores (McKibben and Barnes 1986). The final result is the release of heavy metal ions release following the acid mine drainage. With increased awareness of the need for environmental protection, environmental issues related to pyrite weathering, including acid mine drainage and pollution by heavy metal ions, are currently attracting increasing attention. Therefore, a large number of studies have attempted to discover the processes and mechanisms of pyrite

weathering under natural conditions (Hindshaw et al. 2016; Meng et al. 2016; Droste and Wisotzky 2015; Nordstrom 2015). It is worth pointing out that pyrite weathering is an electrochemical process (Rimstidt and Vaughan 2003). Much research has shown that factors that often affect electrochemical interactions, such as temperature (Lefticariu et al. 2006), the degree of acidity or alkalinity of the solution (Todd et al. 2003), and stress (Liu et al. 2013), as well as external environmental conditions, including glaciation (Hindshaw et al. 2016) and climate (Root et al. 2015; Caraballo et al. 2016), etc., will also affect pyrite weathering. Among these factors, rainfall is one of the important factors that affect pyrite weathering and the accompanying environmental issues, such as AMD and heavy metal ion pollution. On the one hand, rainfall creates an electrolyte medium for pyrite weathering; on the other hand, rainfall facilitates the transfer of ions via water-rock interactions. Yamaguchi et al. (2015) investigated the chemistry and flow of water in an abandoned sulfide mine, taking into account seasonal variations in rainfall. The results show that the water becomes acidic as dissolved oxygen oxidizes pyrite. Along the flow path through the rocks, the redox potential of the water becomes reducing, such that pyrite becomes stable and the pH of the mine drainage becomes neutral. Upon leaving the mine, the drainage becomes acidic again due to the oxidation of pyrite in the rocks. Rainfall affects pyrite mine AMD and the quantities of dissolved elements. Davies et al. (2011) characterized the acid mine drainage in a high rainfall mountain environment. They quantified the AMD and discharge in real time and showed that the runoff from extreme rain events has low pH, showing that water-rock reactions occur on a time scale of minutes to days. Smuda et al. (2007) studied the element mobility from a sulfide-rich waste rock dump called Excelsior, which contains >60 wt% pyrite and <5 wt% calcite/dolomite. The data suggest that, during the dry winter season, rapid evaporation of outcropping pore solutions and the subsequent precipitation of efflorescent salts results in heavy metal enrichment at the base of the Excelsior waste rock dump. During the wet summer season, rain events caused the dissolution of most of the efflorescent salts, removed the enrichment at the base, and resulted in a washout of acid solutions rich in Fe, Mn, Zn, Cu, Cd, As, and S.

Acid rain (acidic deposition) is caused by emissions of SO_2 (principally from fossil-fuel power stations, metal smelters, and other stationary sources) and NO_x (from mobile sources, industrial sources, and power plants) that form sulfuric and nitric acid in precipitation (Likens et al. 1972). Acid rain has been one of the major international environmental issues. It pollutes soil, aquatic ecosystems (Evans et al. 2001; Skjelkvale et al. 2001), and even threatens human health (Gerhardsson et al. 1994). As a particular kind of rainfall, its effect on pyrite weathering will clearly be more serious. Previous studies (Kucha et al. 1996) revealed that acid rain will mobilize metal elements from metal sulfides themselves in sulfide mines. Moreover, where pyrite is a main gold-bearing mineral, the presence of acid rain could lead to the chemical transport and precipitation of gold in anoxic surface waters, reconciling evidence for fluvial deposition with evidence suggesting hydrothermal-like chemical reactions (Heinrich 2015). In nature, pyrite raw ore or contain pyrite sulfide mine tailings are often seen at the surface of the crust or at shallow depths in the crust, and they often suffer acid rain washing. Taking China as an example, in the three famous and large mines where sulfide minerals are extracted from deposits, Fankou (in Guandong Province), Jinding and Dongchuan (in Yunnan Province), the sulfide mineral deposits all lie in areas that experience serious acid rain in China (Zhang et al. 2012).

As mentioned above, studies seldom concentrate on pyrite weathering under acid rain, and previous studies have never characterized the mechanism of pyrite weathering under acid rain conditions. In fact, pyrite weathering is an electrochemical process. Therefore, in this study, the electrochemical behavior of pyrite from an area experiencing serious acid rain pollution, Dongchuan (Yunnan Province, China), under simulated acid rain (SAR) was studied. The primary objectives of this study were (1) to understand the responses of pyrite weathering mechanisms to SAR and (2) to quantitatively investigate the effects of SAR on pyrite weathering.

Experimental methodology

Preparation of pyrite electrodes

Pyrite samples were collected from Dongchuan Pb-Zn mine (Yunnan Province, China). Reflected light microscopy and X-ray diffraction analysis indicated that the samples existed as a pure, homogeneous phase. Electron microprobe analysis confirmed that the Fe and S contents (in wt%) of the pyrite samples are 46.89 and 52.96%, Ni and others are 0.0015 and 0.00485%, respectively. These pyrite samples were also used for soaking study. The pyrite samples were cut into approximately cubic shapes, and their bottom surfaces were guaranteed to represent a working area of 0.25 cm^2. The samples were then connected to a copper wire using silver paint on the upper surface and sealed by epoxy resin, keeping only the working surface exposed to the solution. Munoz et al. (1998) described the electrode preparation method in detail. Prior to each test, the mineral electrode was polished with 1.0-, 0.3-, and 0.05-μm alumina powder in sequence to obtain a fresh surface. The electrode was then degreased using alcohol, rinsed with deionized water, and dried in a stream of air.

Simulated acid rain

According to monitoring data on acid rain from 2005 to 2011 in China, the type of acid rain was mainly sulfuric acid rain, and the contribution of nitrate to precipitation acidity increased each year. The annual pH value was approximately the same as that observed in the USA, as well as in Japan and other East Asian countries. However, the deposition flux of the major acidic ions was at a high level (Xie et al. 2012). This is particularly true in Dongchuan (Yunnan Province, China), one of the areas experiencing serious acid rain in China. According to the Dongchuan Environmental Monitoring Station's monitoring data (An 2015), the average pH of rain in Dongchuan was 4.42~6.51 between 2006 and 2013, and the average proportion of the concentrations (mol/l) of SO_4^{2-} and NO_3^- is 3.39:1. To mimic the characteristics of acid rain in China, especially in Dongchuan, according to the above analysis, first, a dilute solution containing $CaSO_4$, $(NH_4)_2SO_4$, $MgSO_4$, $NaNO_3$, NH_4Cl, NaCl, and KF with a mole ratio of 20:9:5:10:2:2:4 was prepared. In this solution, the mole ratio of SO_4^{2-} to NO_3^- was 3.39:1. Then, three types of acid rain with pH values of 5.6, 4.6, and 3.6 were prepared by adjusting the solution pH with a solution containing H_2SO_4 and HNO_3 with a mole ratio of SO_4^{2-} to NO_3^- of 3.39:1. The detailed ionic composition of the SAR is listed in Table 1.

Electrochemical study

Electrochemical measurements were performed using a computer-controlled electrochemical measurement system (PARSTAT 2273, Princeton Applied Research) with a conventional three-electrode electrolytic cell that included a platinum auxiliary electrode, a pyrite working electrode, and a saturated calomel reference electrode (SCE). All other potentials in this study are quoted relative to the SCE (0.242 V vs. standard hydrogen electrode), unless otherwise stated. To minimize the resistance of the solution between the working electrode and the reference electrode, the reference electrode was connected to a Luggin capillary.

The electrolyte was SAR with a pH of 5.6, 4.6, or 3.6 (refer to "Simulated acid rain" section), respectively, and 25 ml of electrolyte was used in each test. The working, auxiliary and reference electrodes were situated in the same locations in each test to ensure a uniform spatial relationship. The experiments were conducted at 25 ± 1 °C, and this temperature was maintained using a water bath.

Cyclic voltammetry (CV) experiments were carried out at a scan rate of 5 $mV \cdot s^{-1}$. The sweep initiated in the positive direction, and the potential was measured starting from the open circuit potential (OCP, *E*oc) to 0.8 V ($E_{\lambda a}$, vs. SCE). The scan was then reversed to reach −1.2 V ($E_{\lambda c}$, vs. SCE) and was finally returned to the OCP as the final potential (E_f). Polarization curves were obtained by changing the electrode potential automatically from −250 to +250 mV (vs. the *E*oc) at a scan rate of 10 $mV \cdot s^{-1}$. Electrochemical impedance spectroscopy (EIS) tests were performed at the OCP and in the frequency range of 0.001~10,000 Hz with a peak-to-peak amplitude of 10 mV. ZSimpWin 3.20 (2004) software was then used to fit the impedance data. To ensure reproducibility, identical experiments were repeated at least three times to ensure that the reported results were reproducible (i.e., that the random errors of all three identical experimental results were within tolerance), and all the reported results in this study were averaged.

Prior to the CV experiments, polarization curves, and EIS tests, OCP tests were performed. During each OCP test, the electrode potential was increased for 600 s before reaching a quasi-steady-state; the steady-state was defined here as a change of less than 2 mV per 300 s. Then, the electrode was stabilized for 400 s, and the potential was recorded as the OCP. During the second and third identical experiments, if the potential was not within ±5 mV (compared with the first test) at the quasi-steady-state, then the OCP test was terminated, and a new test was performed until the same OCP as the first test was obtained when stabilized for ~400 s.

Table 1 Ions concentrations of simulated acid rain (μmol/l)

pH	Ca^{2+}	NH_4^+	Mg^{2+}	K^+	Na^+	Cl^-	F^-	SO_4^{2-}	NO_3^-
5.6	40	40	10	8	24	8	8	70	21
4.6	40	40	10	8	24	8	8	87	26
3.6	40	40	10	8	24	8	8	262	77

Soaking study

First, the massive pyrite samples were crushed into 20–40 mesh size, and pure pyrite particles were selected out under a microscope; then, these pyrite particles were ground to 200-mesh powder using an agate mortar under ethyl alcohol surrounding conditions; finally, these pyrite powders were dried in a stream of nitrogen and reserved in a vacuum chamber for the subsequent soaking experiments. Nine Erlenmeyer flasks were each filled with 0.5 g of pyrite powder and were divided into three equal groups. Every group SAR was 60 ml, having pH values of 3.6, 4.6, and 5.6, and subjected to a temperature of 25 ± 1, 35 ± 1, and 45 ± 1 °C, respectively. Experimental temperature was conducted by a water bath. The pulp pH was measured every 5 min for the first 30 min after the SAR was poured into each flask, then

every 10 min during the second 30 min, an hour later, and then every 2 days up to 70 days.

Results and discussion

Cyclic voltammetry studies

Figure 1 show the cyclic voltammogram obtained from the pyrite with the sweep potential starting from the open circuit potential, *E*oc. The comparison of the cyclic curves of the pyrite at different acidities and different temperatures showed that they had similar *E-i* profiles, except that the pyrite current changed more strongly under higher temperatures or stronger acidity at the same scan potential, which means that the pyrite had the same electrochemical interaction mechanism under these SAR conditions. In all these cyclic curves, following the potential from OCP to more positive values, the oxidation rate increased quickly. The first anodic current peak A1 occurs at a potential of 0.6–0.65 V. Biegler and Swift (1979), Giannetti et al. (2001), and Antonijevic et al. (2005) noted that it corresponds to the oxidation of pyrite to ferric ions, sulfur, and sulfate as shown in reaction (1).

$$A1: FeS_2 + 8H_2O \rightarrow Fe^{3+} + 2SO_4^{2-} + 16H^+ + 15e^- \quad (1)$$

In the reverse scan, two redox peaks occur. Peak C1 occurs near 0.4 V and corresponds to the reduction of Fe^{3+} as in reaction (2) (Ahlberg and Broo 1997). Peak C2 occurs near −0.4 V and corresponds to the reduction of S^0 as in reaction (3) (Yin et al. 1999). When the potential scan reaches approximately −0.7 V, another redox peak C3 occurs, due to the reduction of pyrite as in reaction (4), which is consistent with the result of Tao et al. (2003). FeS generated in reaction (4) will then dissolve in SAR environments, as in reaction (5).

$$C1: Fe^{3+} + e^- \rightarrow Fe^{2+} \quad (2)$$

$$C2: S^0 + 2H^+ + 2e^- \rightarrow H_2S \quad (3)$$

$$C3: FeS_2 + 2H^+ + 2e^- \rightarrow FeS + H_2S \quad (4)$$

$$FeS + 2H^+ = Fe^{2+} + H_2S \quad (5)$$

As the potential sweep reverses in direction at −1.2 V, the current swings positive at about −0.1 V, and a second anodic peak A2 can be observed. This peak is attributed to the oxidation of H_2S (Nava et al. 2002), where the H_2S is produced during the cathodic sweep as in reactions (3), (4), and (5).

$$A2: H_2S \rightarrow S^0 + 2H^+ + 2e^- \quad (6)$$

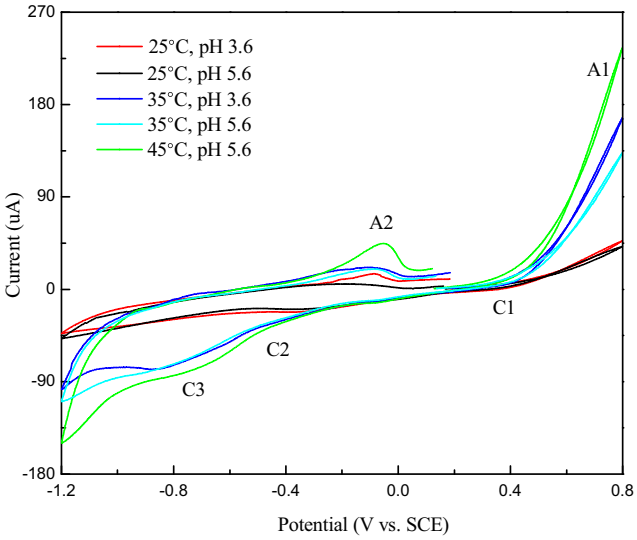

Fig. 1 Typical cyclic voltammograms obtained on pyrite electrode in different acidities and temperatures SAR solutions. $E_i = E_{OC}$, $E_{\lambda a} = 0.8$ V, $E_{\lambda c} = -1.2$ V, $E_f = E_{OC}$, $v = 5$ mV·s^{-1}

Polarization curve studies

Figure 2 shows the polarization curves of the pyrite electrode using SAR with pH values of 3.6, 4.6, and 5.6 under different temperatures at a scan rate of 10 mV·s^{-1}. All these polarization curves display a similar *E-i* profile, which means the pyrite has the same electrochemical interaction mechanism under these conditions. Moreover, there are two obvious tendencies, which are as follows. Decreasing the pH at the same temperature, or increasing the temperature at the same pH, will cause these curves shift toward higher densities of current and lower values of potential. These results are consistent with the tendency of the CV curves.

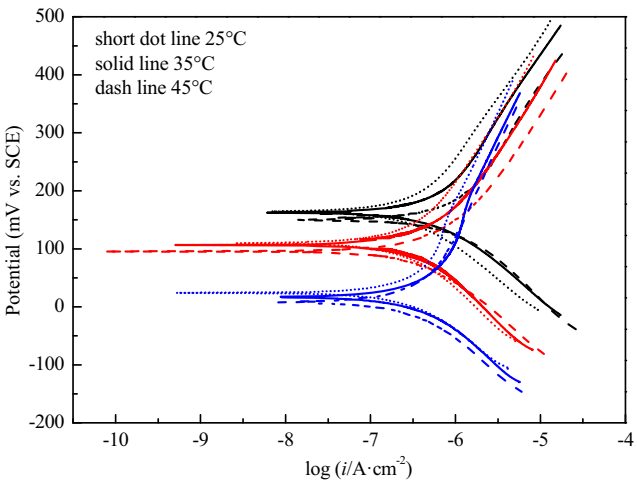

Fig. 2 Potential-time relationships of pyrite electrode in pH 3.6 (*black lines*), pH 4.6 (*red lines*), and pH 5.6 (*blue lines*) SAR under different temperatures

For the electrochemical analyses, the first and most important parameters are the corrosion current density (i_{corr}) and corrosion potential (E_{corr}). The parameter i_{corr} reflects the corrosion rate of the material. Specifically, the higher the density of current is, the faster the corrosion rate will be, while E_{corr} is related to the corrosion possibility of the material. A negative value of E_{corr} means the material is difficult to corrode. The i_{corr}, E_{corr}, including Tafel slopes of anode (b_a) and cathode (b_c) can observe from the polarization curves based on the extrapolation methods (Bard and Faulkner 2001). Furthermore, the polarization resistance, R_p, can be calculated from the Stern-Geary equation $R_p = b_a b_c/[2.3\ i_{corr}\ (b_a + b_c)]$ (Stern and Geary 1957). The experimentally determined polarization results for the pyrite electrode under SAR of different acidities and at different temperatures are summarized in Tables 2 and 3, respectively.

The influence of SAR acidity

When pyrite suffered erosion by SAR at the same temperature, such as at 25, 35, or 45 °C, the polarization results (Table 2) suggest that the pyrite has a similar tendency, i.e., the i_{corr} of the pyrite increases and the E_{corr} becomes more positive as SAR acidity increases. As previously mentioned, a larger value of i_{corr} indicates a large corrosion rate, and a positive value of E_{corr} indicates that corrosion is more difficult. All these results showed that increasing acidity promotes the electrochemical corrosion of pyrite. These phenomena can be explained in that, at these SAR conditions, the pyrite acted as the anode and was oxidized as in reactions (7). S^0 was produced and absorbed onto the pyrite's surface. Obviously, stronger acidity is favorable for S^0 dissolution; furthermore, the pyrite corrosion potential became more positive as the acidity of the SAR increased. Higher corrosion potential would lead to pyrite anode dissolution (Alloway and Ayres 1998). These two causes led the Tafel slope of the anode (b_a) to decrease dramatically when the acidity of the SAR increased, indicating that the pyrite anodic oxidization process was accelerated. At the cathode, O_2 was reduced as in reaction (8). According to reaction (8), increases in the concentration of H^+ seem favorable for the cathodic reduction of O_2. However, it remains a fact that, following increases in the concentration of H^+, the SO_4^{2-} and NO_3^- concentrations of the simulated acid rain also increase, resulting in a decrease in the solubility of the oxygen (Moslemi et al. 2011), which is unfavorable for cathodic reduction of O_2. Therefore, the corollary of the above is that the Tafel slope of the cathode (b_c) first increases and then decreases in this work. To overcome these two Tafel slopes, the general result is that the polarization resistance R_p decreases. That is, increases in acidity promote the electrochemical corrosion of pyrite. The promotion efficiency (η) was 3.12 and 8.48%, 31.14 and 40.23%, as well as 53.74 and 104.29%, respectively, corresponding to increases in acidity from 5.6 to 4.6 and then to 3.6 at 25, 35, and 45 °C, respectively. The promotion efficiency is defined by $\eta = \left(i_{corr} - i^0_{corr}\right) / i^0_{corr} \times 100\%$, which is often used as the inhibition efficiency in materials science (Solmaz et al. 2008; Wang et al. 2011). Comparing these promoting efficiencies, we can observe that environmental temperature has an important effect on pyrite weathering, even when pyrite suffers erosion under SAR with the same acidity. The higher the environmental temperature is, the bigger the promoting efficiency will be when the SAR experiences the same acidity increase. Specifically, the largest promotion efficiency reached 104.29% at 45 °C when the SAR acidity increased from pH 5.6 to pH 3.6.

$$Anode: FeS_2 \rightarrow Fe^{2+} + 2S^0 + 2e^- \quad (7)$$

$$Cathode: O_2 + 4H^+ + 4e^- \rightarrow 2H_2O \quad (8)$$

The influence of temperature

When pyrite suffered erosion under SAR with the same acidity, such as pH values of 3.6, 4.6, and 5.6, the polarization results (Table 3) suggest that the pyrite has a similar tendency,

Table 2 Electrochemical parameters of the pyrite electrode in SAR at a same different and different pH values

Temperature (°C)	pH	E_{corr} (mV)	i_{corr} (μA·cm^{-2})	b_c (mV)	b_a (mV)	R_p (Ω·cm^2)	η (%)
25	5.6	24.0	0.448	135.8	381.6	9.72×10^4	
	4.6	110.1	0.462	160.5	280.6	9.60×10^4	3.12
	3.6	164.5	0.486	140.2	255.2	8.09×10^4	8.48
35	5.6	19.7	0.517	143.6	358.3	8.62×10^4	
	4.6	107.6	0.678	204.0	268.8	7.43×10^4	31.14
	3.6	162.8	0.725	126.9	243.1	5.00×10^4	40.23
45	5.6	7.9	0.536	148.6	355.8	8.50×10^4	
	4.6	95.5	0.824	216.4	256.7	6.19×10^4	53.74
	3.6	150.3	1.095	117.5	240.3	3.13×10^4	104.29

Table 3 Electrochemical parameters of the pyrite electrode in SAR at a same pH value and different temperatures

pH	Temperature (°C)	E_{corr} (mV)	i_{corr} (μA·cm^{-2})	b_c (mV)	b_a (mV)	R_p (Ω·cm^2)	η (%)
3.6	25	164.5	0.486	140.2	255.2	8.09×10^4	
	35	162.8	0.725	126.9	243.1	5.00×10^4	49.17
	45	150.3	1.095	117.5	240.3	3.13×10^4	125.31
4.6	25	110.1	0.462	160.5	280.6	9.60×10^4	
	35	107.6	0.678	204.0	268.8	7.43×10^4	46.75
	45	95.5	0.824	216.4	256.7	6.19×10^4	78.35
5.6	25	24.0	0.448	135. 8	381.6	9.72×10^4	
	35	19.7	0.517	143.6	358.3	8.62×10^4	15.40
	45	7.9	0.536	148.6	355.8	8.50×10^4	19.64

i.e., the i_{corr} of pyrite increases and the E_{corr} becomes more negative as the SAR temperature increases. These results also revealed that increases in temperature promote the electrochemical corrosion of pyrite. These phenomena can be explained by the following. At the anode (reaction (7)), the clearly higher temperature causes the conversion of internal energy into electrochemical energy, which is unfavorable for the development of a S^0 cover on the pyrite surface, and hence causes the Tafel slope of the anode (b_a) to decrease, i.e., the anodic polarization resistance of the pyrite decreased. To the cathode reaction, the increase in temperature causes two different effects. The higher temperature accelerates O_2 diffusion and hence promotes the cathodic reduction of O_2, and in reverse leads to a decrease in dissolved oxygen, weakening the cathodic reduction of O_2. The final results of the effects of temperature coupled to the dissolved oxygen are as follows. (1) The effect of O_2 diffusion is dominant when the SAR has a high acidity (pH 3.6 in this work). This is because a high concentration of H^+ ions causes a drop in dissolved oxygen. Clearly, a low concentration of O_2 is advantageous for its diffusion, and this is why the Tafel slope of the cathode (b_c) is reduced at pH 3.6 when the temperature increases from 25 to 35 °C and finally to 45 °C. (2) The effect of dissolved oxygen becomes less dominant when the SAR has a low acidity (pH 4.6 and pH 5.6). The reason is, compared with high acidity SAR (pH 3.6), the concentration of dissolved oxygen at low acidity (pH 4.6 and pH 5.6) is bigger. Obviously, the greater concentration of dissolved oxygen is unfavorable for its diffusion, which results in an increase in the Tafel slope of the cathode (b_c) when the temperature increases from 25 to 35 °C and finally to 45 °C. To overcome these two Tafel slopes, the general result is the polarization resistance R_p decreases, that is, increasing temperature promotes the electrochemical corrosion of pyrite at the same acidity. The promotion efficiencies were 49.17 and 125.31%, 46.75 and 78.35%, as well as 15.40 and 19.64%, respectively, corresponding to the temperature increased from 25 to 35 °C and finally to 45 °C at pH values of 3.6, 4.6, and 5.6, respectively. Comparing the estimated promotion efficiency, we can also observe that the SAR acidity has an important effect on the weathering of pyrite when the pyrite experiences the same environmental temperature. The more acidic the SAR is, the bigger the promotion efficiency will be when the environmental temperature increases at the same acidity. In particular, the greatest promotion efficiency in this work, 125.31%, was achieved at a pH of 3.6 when the environmental temperature increased from 25 to 45 °C.

Electrochemical impedance spectroscopy study

EIS is one of several effective electrochemical techniques that can reveal the characteristics of electrodes and electrochemical reactions.

Figure 3 shows the Bode (a) and Nyquist plots (b) for pyrite at the OCP at different SAR acidities and temperatures. The Bode plots reflect two time constants and the Nyquist plots resemble distorted capacitive loops suggest two capacitive loops. The first, which is obtained at high frequencies, is attributed to the charge transfer resistance (R_t) that corresponds to the resistance between the pyrite and the outer Helmholtz plane. The second, which is obtained at low frequencies, is related to the combination of pseudo-capacitance impedance (due to the passive layer) and a resistance R_p. The deviation from an ideal semicircle is generally attributed to frequency dispersion, as well as to the inhomogeneities of the passive layer surface. The related electrochemical equivalent circuit (EEC) used to model the pyrite/electrolyte interface is shown in Fig. 3c, where R_s is the resistance of the electrolyte and other ohmic resistance, R_t is the charge transfer resistance, R_p is the film resistance, CPE_{dl} represents the constant phase element that replaced the double layer capacitance, and CPE_p represents the constant phase element that replaced the passive film capacitance (C_p).

The impedance parameters for the pyrite electrode under SAR of different acidities and different temperatures are presented in Tables 4 and 5.

When pyrite corrodes in SAR at the same temperature (25 °C), the impedance parameters shown in Table 4 show

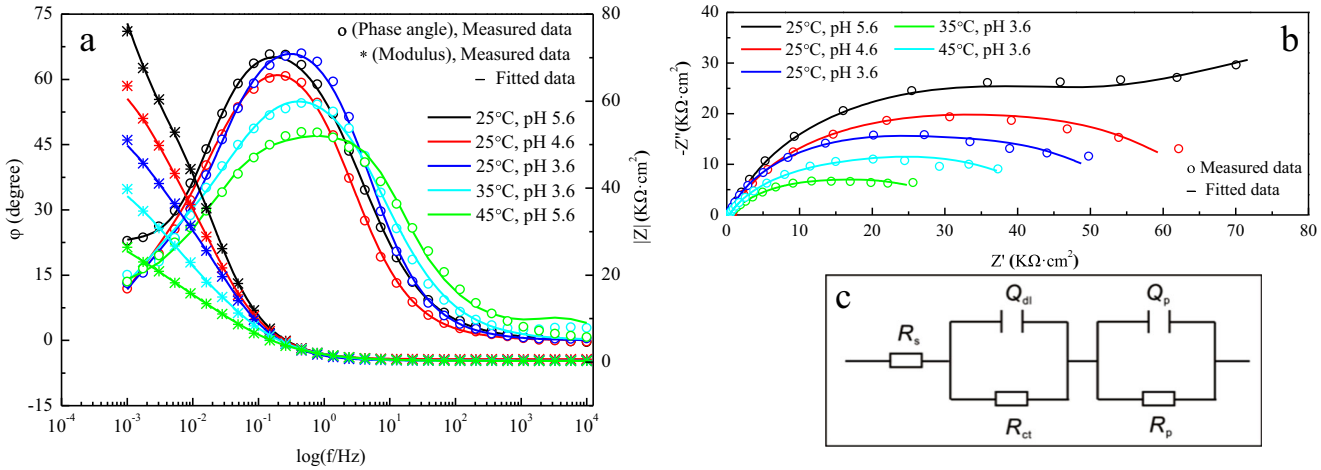

Fig. 3 Bode plots (**a**), Nyquist plots (**b**), and equivalent circuit (**c**) of the pyrite electrode in different acidities and temperatures SAR solutions

that increased acidity results in decreases in the charge transfer resistance (R_t) and the passivation resistance (R_p), which means that increased acidity is favorable for charge transfer at the double layer and makes it difficult to form a passivation film. These are the causes that explain why increases acidity prompts pyrite weathering, which is in agreement with the polarization curve results. When acidity increased from pH 5.6 to 4.6 and then to 3.6, note that the rates of pyrite charge transfer resistance decrease η_t (η_t is defined as $\eta_t = \left(R_t - R_t^0\right)/R_t^0 \times 100\%$) were 77.58 and 80.45%, whereas the rates of passivation film resistance decrease η_p (η_p is defined as $\eta_p = \left(R_p - R_p^0\right)/R_p^0 \times 100\%$) were 22.46 and 30.26%, respectively. These results reveal the main cause by which increased acidity prompts pyrite weathering; that is, it dramatically decreases the charge transfer resistance. As one of the reactants, the effect of H^+ is realized mainly through the double layer effect, which corresponds to the mechanism described by reaction (8).

When pyrite suffers corrosion in SAR of the same acidity (pH 3.6), the impedance parameters shown in Table 5 show that increased temperature cause decreases in the charge transfer resistance (R_t) and the passivation resistance (R_p), which means increased temperature favors charge transfer at the double layer and makes it difficult to form a passivation film. As a result, when temperature increased from 25 to 35 °C and then to 45 °C, the rates of charge transfer resistance (η_t) decrease for pyrite were 9.69 and 33.33%, and the rates of passivation film resistance (η_p) decrease were 45.09 and 51.19%, respectively. These results reveal the main cause by which increases in temperature prompt pyrite weathering; that is, the passivation film resistance dramatically decreases. In other words, increased environmental temperature mainly disadvantageous for passivation film formation and hence accelerates pyrite weathering.

Soaking

In this section, to what extent the environmental temperature and the acidity of acid rain affect pyrite weathering, especially in terms of their ability pyrite release H^+ ions, was investigated. Figure 4 shows the dynamic pH changes of 0.1 g (200-mesh) pyrite pulp in a 60-ml different acidities (pH 5.6, 4.6, or 3.6) and temperatures (25, 35, or 45 °C) SAR solutions. The nine dynamic pH curves show three stages similar varying tendency, the first stage, the pyrite pulp pH had a "sharply" decrease at the initial no more than 60 min acid rain erodes, the second stage, the pyrite pulp pH had a "dramatically" decrease, and the third stage is changed to flatten. Detailed tendency of the three stages are shown as following.

The first stage, the pyrite pulp had a "sharply" decrease at the initial 60 min when they soaked in the SAR solution, here, the "sharply" is defined as pH falling range exceed 0.1 per hour, no matter the SAR acidity or environmental temperature. This is because that when 0.1 g 200-mesh pyrite particles were soaked in 60 ml acid rain, the pyrite was oxidized as

Table 4 Equivalent circuit model parameters for pyrite in SAR at 25 °C and under different acidities

pH	R_t (Ω·cm²)	η	R_p (Ω·cm²)	η
5.6	1.32×10^5		4.23×10^4	
4.6	2.96×10^4	77.58	3.28×10^4	22.46
3.6	2.58×10^4	80.45	2.95×10^4	30.26

Table 5 Equivalent circuit model parameters for pyrite in pH 3.6 SAR at different temperatures

Temperature (°C)	R_t (Ω·cm²)	η	R_p (Ω·cm²)	η
25	2.58×10^4		2.95×10^4	
35	2.33×10^4	9.69	1.62×10^4	45.09
45	1.72×10^4	33.33	1.44×10^4	51.19

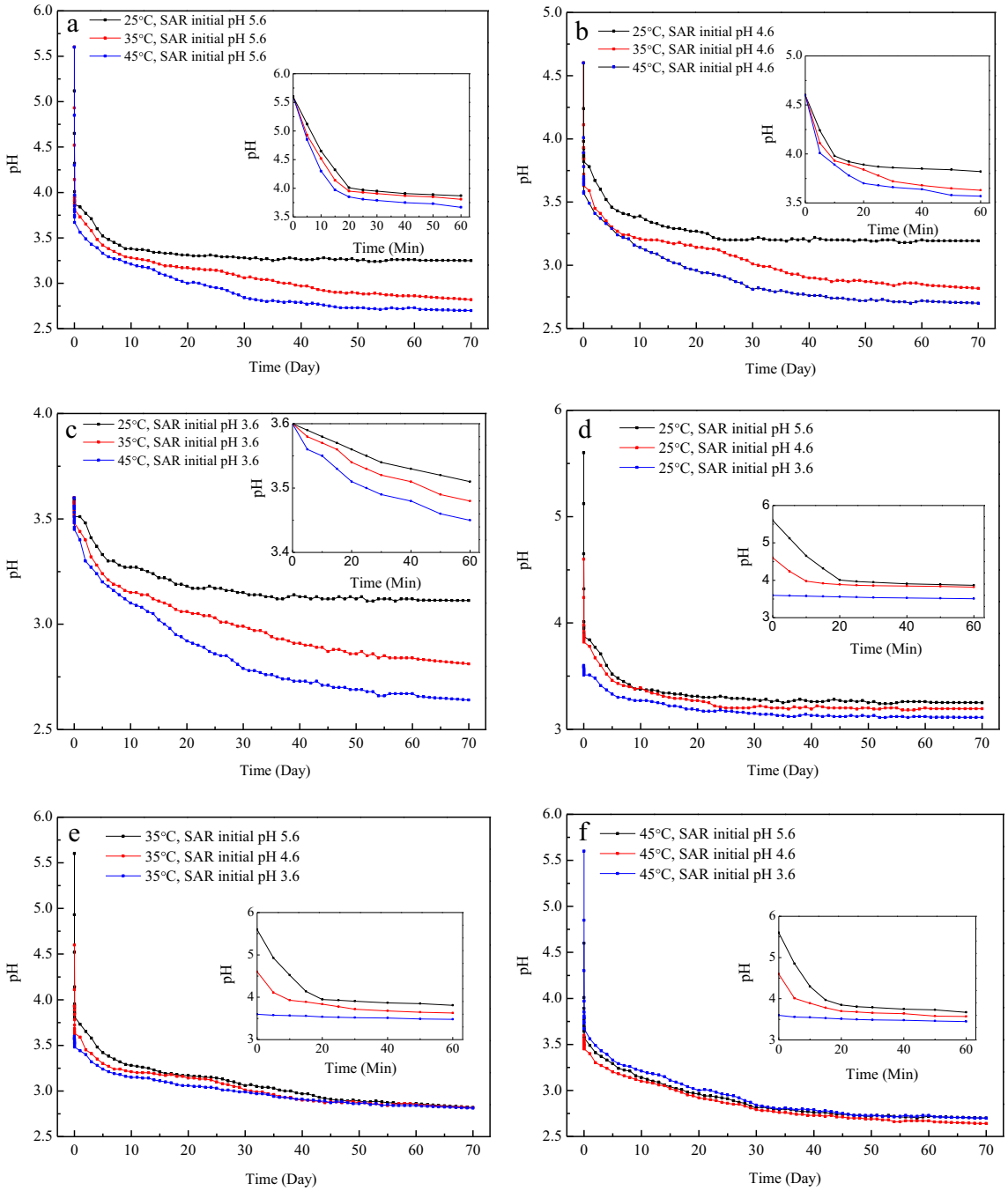

Fig. 4 pH-time relationships of pyrite pulp in different acidities and temperatures SAR solutions

reaction (7) and released off H^+ ions, as for the pyrite particles was 200-meshes, i.e., the total surface area of the 0.1 g pyrite surface would be very large, the pyrite particles and the dissolved oxygen in the SAR would have sufficient contact area, and hence set out large number of H^+ ions in a shorty time to the 60 ml solution. The pyrite pulp pH values in different acidities and temperatures SAR are show in Table 6. From this table we can see, when the pyrite particles are in an identical environmental temperature, a smaller pH acid rain cause a smaller pulp, while when pyrite particles eroded by a same

Table 6 The pyrite pulp pH after soak 60 min in different acidities and temperatures SARs

SAR pH	Temperature (°C)		
	25	35	45
5.6	3.87	3.81	3.67
4.6	3.82	3.63	3.57
3.6	3.51	3.48	3.45

Table 7 The pyrite pulp pH values and the number of days that the pulp terminated "dramatically" decreased in different acidities and temperatures SARs

SAR pH	pH			Time (day)		
	25 °C	35 °C	45 °C	25 °C	35 °C	45 °C
5.6	3.84	3.17	2.81	9	30	43
4.6	3.30	3.00	2.78	25	41	48
3.6	3.17	2.93	2.73	31	46	53

acidity acid rain, the higher environmental temperature resulted in a smaller pulp pH after eroded 60 min. These results reveal that strong acidity or high environmental temperature accelerate the pyrite weathering and cause it to release more H^+ ions. The biggest and smallest pulp pH values were 3.87 and 3.45, respectively, and these values correspond to a SAR pH of 3.6 at 45 °C and a SAR pH of 5.6 at 25 °C. All these results agree well with previously measured electrochemical results.

During the second stage, the pyrite pulp displayed a "dramatic" decrease. Here, a "dramatic" decrease is defined as a rate of decrease in pH exceeding 0.01 per day. The cause was that S^0 was produced and adsorbed onto the pyrite article surfaces, which decreased the pyrite surface. Detailed pyrite pulp pH values and the number of days after which the pulp terminated its "dramatic" decrease are shown in Table 7. The results show that, when pyrite erodes in acid rain media, the "dramatic" decrease stage changed more permanently when acid rain had a stronger acidity or occurred at a higher temperature. Furthermore, the pyrite pulp had a smaller pH at the terminated stage. In this work, the pyrite pulp "dramatic" decrease days were 9 and 53 days, and their terminated stage pH values were 3.84 and 2.73, respectively, for pH values and temperatures of 5.6 and 25 °C and 4.6 and 45 °C, respectively.

During the third stage, the pulp pH decreased only slightly. The cause is that, with more and more S^0 produced by pyrite oxidation (reaction (7)), this species would cover the pyrite surface and form a passivation membrane, thereby inhibiting pyrite oxidation. When the pyrite articles suffered erosion from acid rain at an identical acidity, the higher environmental temperature caused a smaller pulp pH during the measured 70 days (Table 8). In particular, when the environmental temperature increased by 10 °C, the terminal pulp pH has obviously decreased, meaning that increased temperature clearly results in accelerated pyrite corrosion and the release of additional H^+ ions. These results were in agreement with previous electrochemical results. When the pyrite articles suffered erosion in acid rain at the same temperature, the higher acidity acid rain led to a smaller pulp pH at 25 °C, whereas the acidity of the acid rain did not have an obvious effect at 35 and 45 °C during this stage. These observations could be explained by the decrease in dissolved oxygen with increasing acid rain

Table 8 The pyrite pulp pH values that the pulp slowly decreased in different acidities and temperatures SARs during the measured 70 days

SAR pH	Temperature (°C)		
	25	35	45
5.6	3.25	2.82	2.69
4.6	3.19	2.82	2.70
3.6	3.11	2.81	2.64

acidity (leading to larger contents of SO_4^{2-} and NO_3^-, as previously explained). In particular, at higher temperatures (such as 35 or 45 °C in this work), the dissolved oxygen changed by a smaller amount. When pyrite is at these high temperatures, acid rain that has a stronger acidity (such as pH 3.6 in this work) might be thought to enhance pyrite corrosion; unfortunately, a decrease in oxygen in the acid rain inhibits pyrite corrosion. Note that the S^0 passivation film is not a terminal product; it will gradually transform into SO_4^{2-} in acidic environments as time passes.

Implication for sulfide mine environments

In a sulfide mineral mine that is in a region affected by acid rain, the exposed, raw pyrite ore or tailings will suffer acid rain erosion, causing mine drainage of higher acidity, regardless of the acid rain's acidity. Acid rain with higher acidity results in serious acid mine drainage pollution. Environmental temperature greatly influences pyrite weathering, meaning that the latitude, elevation, and season have substantial influence on pyrite weathering. Generally, when sulfide mines are at low latitudes or in low elevation regions, as well as during warmer seasons, higher temperatures occur and will intensify the weathering of pyrite, causing more serious environmental pollution.

Conclusions

Based on the established electrochemical parameters and the dynamic changes in pH and pyrite behavior in simulated acid rain of different acidities and at different environmental temperatures, the following conclusions can be derived:

(1) Cyclic curve studies revealed that pyrite has the same electrochemical interaction mechanism under different simulated acid rain conditions, regardless of acidity or environmental temperature.
(2) Polarization curve studies revealed that either more acidic acid rain or higher environmental temperatures can accelerate pyrite corrosion. Within the investigated ranges of acidity (pH 5.6~3.6) and temperature (25 °C~45 °C), compared with conditions including

temperatures of 25 °C and an acid rain pH of 5.6, the pyrite weathering prompt efficiency reached 104.29% as the acid rain pH increased from 5.6 to 3.6, and 125.31% as the environmental temperature increased from 25 to 45 °C when the other conditions were kept the same. Measurements made using EIS revealed that the main causes were a dramatic decrease in the charge transfer resistance and the passivation film resistance.

(3) Acid rain causes higher acidity mine drainage, regardless of the acid rain acidity and environmental temperature. Furthermore, stronger acidity or higher environmental temperatures cause serious acid drainage. The natural parameters of latitude, elevation, and season have considerable influence on pyrite weathering, because temperature is an important influencing factor.

Acknowledgments This work was financially supported by the 135 Program of the Institute of Geochemistry, CAS, and the 863 High Technology Research and Development Program of China (2010AA09Z207).

References

Ahlberg E, Broo AE (1997) Electrochemical reaction mechanisms at pyrite in acidic perchlorate solutions. J Electrochem Soc 144: 1281–1286

Alloway BJ, Ayres D (1998) Chemical principles of environmental pollution. Water Air Soil Poll 102(1–2):216–218

An CH (2015) Acid rain and its control in Dongchuan. Environ Sci Surf 34(1):45–49 (In Chinese with English abstract)

Antonijevic MM, Dimitrijevic MD, Serbula SM, Dimitrijevic VLJ, Bogdanovic GD, Milic SM (2005) Influence of inorganic anions on electrochemical behaviour of pyrite. Electrochim Acta 50: 4160–4167

Bard AJ, Faulkner LR (2001) Electrochemical methods: fundamentals and applications, 2nd. Wiley and Sons, Hoboken

Biegler T, Swift DA (1979) Anodic behaviour of pyrite in acid solutions. Electrochim Acta 24:415–420

Caraballo MA, Macías F, Nieto JM, Ayora C (2016) Long term fluctuations of groundwater mine pollution in a sulfide mining district with dry Mediterranean climate: implications for water resources management and remediation. Sci Total Environ 539:427–435

Davies H, Weber P, Lindsay P, Craw D, Pope J (2011) Characterisation of acid mine drainage in a high rainfall mountain environment, New Zealand. Sci Total Environ 409(15):2971–2980

Donato PD, Mustin C, Benoit R, Erre R (1993) Spatial distribution of iron and sulphur species on the surface of pyrite. Appl Surf Sci 68(1):81–93

Droste B, Wisotzky F (2015) Pyrite oxidation processes in cretaceous sedimentary rock. Grundwasser 20(3):197–208

Evans CD, Cullen JM, Alewell C, Kopácek J, Marchetto A, Moldan F, Prechtel A, Rogora M, Veselý J, Wright RF (2001) Recovery from acidification in European surface waters. Hydrol Earth Syst Sci 5: 283–297

Gerhardsson L, Oskarsson A, Skerfving S (1994) Acid precipitation—effects on trace elements and human health. Sci Total Environ 153(3):237–245

Giannetti BF, Bonilla SH, Zinola CF, Raboczkay T (2001) A study of the main oxidation products of natural pyrite by voltammetric and photoelectrochemical responses. Hydrometallurgy 60:41–53

Heinrich CA (2015) Witwatersrand gold deposits formed by volcanic rain, anoxic rivers and Archaean life. Nat Geosci 8:206–209

Hindshaw RS, Heaton THE, Boyd ES, Lindsay MR, Tipper ET (2016) Influence of glaciation on mechanisms of mineral weathering in two high Arctic catchments. Chem Geol 420:37–50

Ivanova TA, Matveeva TN, Chanturia VA, Ivanova EN (2015) Composition of multicomponent heracleum extracts and its effect on flotation of gold-bearing sulfides. J Min Sci 51(4):819–824

Kucha H, Martens A, Ottenburgs R, Vos WD, Viaene W (1996) Primary minerals of Zn-Pb mining and metallurgical dumps and their environmental behavior at Plombières, Belgium. Environ Geol 27(1):1–15

Lefticariu L, Pratt LM, Ripley EM (2006) Mineralogic and sulfur isotopic effects accompanying oxidation of pyrite in millimolar solutions of hydrogen peroxide at temperatures from 4 to 150°C. Geochim Cosmochim Acta 70(19):4889–4905

Likens GE, Bormann FH, Johnson NM (1972) Acid rain. Environment 14(2):33–40

Liu QY, Zhang YQ, Li HP (2013) Pressure solution of electrically conductive minerals in shallow crust-galvanic processes: a case study from pyrite under differential stress. Appl Geochem 29:144–150

McKibben MA, Barnes HL (1986) Oxidation of pyrite in low temperature acidic solutions: rate laws and surface textures. Geochim Cosmochim Acta 50:1509–1520

Meng QP, Zhang W, Zhang J, Zhang ZY, Wu TR (2016) Heavy mineral analysis to identify sediment provenance in the Dan River drainage, China. Geosci J 20(4):449–462

Mihajlović L, Nikolić-Mandić S, Vukanović B, Mihajlović R (2009) Use of the sulfide minerals pyrite and chalcopyrite as electrochemical sensors in non-aqueous solutions. The potentiometric titration of weak acids in alcohols. Open Chem 7(4):900–908

Mitsunobu S, Zhu M, Takeichi Y, Ohigashi T, Suga H, Jinno M, Makita H, Sakata M, Ono K, Mase K, Takahashi Y (2016) Direct detection of Fe(II) in extracellular polymeric substances (EPS) at the mineral-microbe interface in bacterial pyrite leaching. Microbes Environ 31(1):63–69

Moslemi H, Shamsi P, Habashi F (2011) Pyrite and pyrrhotite open circuit potentials study: effects on flotation. Miner Eng 24:1038–1045

Munoz JA, Gomez C, Ballester A, Blazquez ML, Gonzalez F, Figueroa M (1998) Electrochemical behaviour of chalcopyrite in the presence of silver and *Sulfolobus* bacteria. J Appl Electrochem 28(1):49–56

Nava JL, Oropeza MT, Gonzalez I (2002) Electrochemical characterisation of sulfur species formed during anodic dissolution of galena concentrate in perchlorate medium at pH 0. Electrochim Acta 47: 1513–1525

Nicol MJ (2016) Photocurrents at chalcopyrite and pyrite electrodes under leaching conditions. Hydrometallurgy 163:104–107

Nordstrom DK (2015) Baseline and premining geochemical characterization of mined sites. Appl Geochem 57:17–34

Peters E, Majima H (1968) Electrochemical reactions of pyrite in acid perchlorate solutions. Can Metal Quart 7:111–117

Rabieh A, Albijanic B, Eksteen JJ (2016) A review of the effects of grinding media and chemical conditions on the flotation of pyrite in refractory gold operations. Miner Eng 94:21–28

Reinholz EL, Roberts SA, Apblett CA, Lechman JB, Schunk PR (2016) Composition and manufacturing effects on electrical conductivity of Li/FeS2 thermal battery cathodes. J Electrochem Soc 163(8): A1723–A1729

Rimstidt JD, Vaughan DJ (2003) Pyrite oxidation: a state-of-the-art assessment of the reaction mechanism. Geochim Cosmochim Acta 67(5):873–880

Root RA, Hayes SM, Hammond CM, Maier RM, Chorover J (2015) Toxic metal(loid) speciation during weathering of iron sulfide mine tailings under semi-arid climate. Appl Geochem 62(SI):131–149

Simic Z, Stanic Z, Milan A (2010) Use of sulphide minerals as electrode sensors for acid-base potentiometric titrations in non-aqueous

solvents and their application for the determination of certain biologically active substances. Sens Lett 8(6):784–791

Skjelkvale BL, Mannio J, Wilander A, Andersen T (2001) Recovery from acidification of lakes in Finland, Norway and Sweden 1990-1999. Hydrol Earth Syst Sci 5:327–337

Smuda J, Dold B, Friese K, Morgenstern P, Glaesser W (2007) Mineralogical and geochemical study of element mobility at the sulfide-rich Excelsior waste rock dump from the polymetallic Zn-Pb-(Ag-Bi-Cu) deposit, Cerro de Pasco, Peru. J Geochem Explor 92(2–3):97–110

Solmaz R, Kardaş G, Yazıcı B, Erbil M (2008) Adsorption and corrosion inhibitive properties of 2-amino-5-mercapto-1, 3, 4-thiadiazole on mild steel in hydrochloric acid media. Colloid Surf A-Physicochem Eng Asp 312:7–17

Stanić Z, Dimić T (2013) Natural mineral pyrite and analytical application thereof in precipitation titrations in non-aqueous solvents. New J Chem 37:3612–3619

Stern M, Geary AL (1957) Electrochemical polarization. 1. A theoretical analysis of the shape of polarization curves. J Electrochem Soc 104: 56–63

Tao DP, Richardson PE, Luttrell GH, Yoon RH (2003) Electrochemical studies of pyrite oxidation and reduction using freshly-fractured electrodes and rotating ring-disc electrodes. Electrochim Acta 48: 3615–3623

Todd EC, Sherman DM, Purton JA (2003) Surface oxidation of pyrite under ambient atmospheric and aqueous (pH 2 to 10) conditions: electronic structure and mineralogy from X-ray absorption spectroscopy. Geochim Cosmochim Acta 67(5):881–893

Wang X, Yang H, Wang F (2011) An investigation of benzimidazole derivative as corrosion inhibitor for mild steel in different concentration HCl solutions. Corros Sci 53:113–121

Xiao L, Chen B, Zhong H, Guo QW (2013) Electro-generation of the microbe fuel cell for pyrite-MnO_2 in the presence of *Acidithiobacillus ferrooxidans*. Appl Mechan Mater 373-375: 2030–2033

Xie SY, Wang RB, Zheng HH (2012) Analysis on the acid rain from 2005 to 2011 in China. Environ Monitor Forewarn 4(5):33–37 (In Chinese with English abstract)

Yamaguchi K, Tomiyama S, Metugi H, Ii H, Ueda A (2015) Flow and geochemical modeling of drainage from Tomitaka mine, Miyazaki, Japan. J Environ Sci 36:130–143

Yin Q, Kelsall GH, Vaughan DJ, Welham NJ (1999) Rotating ring (Pt)-disc (FeS_2) electrode behavior in hydrochloric solutions. Colloid Interf Sci 210:375–383

Zhang XY, Jiang H, Jin JX, Xu XH, Zhang QX (2012) Analysis of acid rain patterns in northeastern China using a decision tree method. Atmos Environ 46(1):590–596